(Online) ISSN 2303-4521
Periodicals of Engineering and Natural Sciences *Original Research*
Vol. 13, No. 4, December 2025, pp.1009-1022

Evaluation of 316L deposition parameters for the reducing stair-case effect of laminated parts by coaxial laser powder deposition

Nicolas Orejarena-Osorio[1], C. L. Sandoval Rodriguez[1]
[1] Faculty of Natural Sciences and Engineering, Unidades Tecnológicas de Santander, Colombia

*Corresponding author E-mail: norejarena@correo.uts.edu.co

ABSTRACT

The time reduction to manufacture tools is a requirement, especially those that due to their operating conditions are subjected to stress, abrasion and wear, as well as having to adapt to new design requirements such as complex shapes and internal cooling channels, which are difficult to machine by conventional processes. In consequence, laminated tools might be a solution, nevertheless, the staircase effect in curved contours appears. This study analyzes the reduction of the staircase effect by coaxial laser deposition of 316L metal powder. Using previously cut sheets with thicknesses of 0.5, 1 and 2 mm, these are stacked to make samples with a 14 mm radius contour. An experiment is then designed, based on Taguchi, to determine the optimal multilayer deposition parameters of the molten metal powder. Parameters such as laser power, overlap, feed rate, substrate thickness and mass flow are considered to determine the lowest roughness measured mechanically and optically. Residual stresses are also analyzed and stacking and deposition strategies are proposed to achieve the desired curvature.

Finally, the staircase effect is reduced and the optimal parameters are obtained, which include higher laser power and feed rate but low mass flow and overlap. In addition, lower roughness is obtained with lower mass flow rate and higher feed rate. Residual tensile stresses are also obtained due to the high cooling rates.

Keywords: Laser powder deposition, staircase effect, laminated parts, metal powder, additive manufacturing, LDMD

1. Introduction

In product development, the manufacture of tools is time consuming and specifically, in metal forming processes, tools are under friction, temperature and high loads. On the one hand, these lead to wear and constant repairs, but on the other hand, they are constantly adapted to the requirements of the final product. In that sense, layered manufacturing is an alternative for time reduction and versatility in redesign and remanufacturing [1]. It has been applied in injection molds, however, the need to improve surface finishes has arisen for instance due to the staircase effect.

Considering this need for additional processes, rapid manufacturing technologies emerged, which include additive, subtractive and hybrid processes [1], where hybrid manufacturing consists of combining additive and subtractive processes, in other words, adding and removing material. In this way, geometry become more flexible and the surface finish are improved. The authors [2] [1] propose the decomposition of a die by layers and their subsequent bonding to reduce time, costs and even the use of different materials to improve properties in different sections of the tool. However, there is a risk of delamination failure. In further work, the author Walczyk et al, [3] proposed the Profiled Edge Laminas (PEL) method for thermoforming tools manufacturing because of its advantages over conventional manufacturing with respect to cooling channels, vacuum channels and embedded sensors. Before assembly, the sheets were individually pre-machined using 2D abrasive waterjet

(AWJ) and once assembled, the surface was CNC machined. However, this process required 2 to 5 times more time than the traditional CNC process.

Other research on laminated tools was the work done by Yoon and Na [4], who made a mold from 1 mm low-carbon steel sheets for an automatic gear shift knob. The sheets were cut and subsequently joined by furnace brazing and dip soldering, determining their optimum parameters and partially reducing the staircase effect. Additional 5-axis machining was required, concluding that machining time was increased compared to conventional machining. In later work [5], the authors proposed that the reduction of the staircase effect can be improved by calculating the right amount of metal wire to fill each step and the correct tilt angle with respect to the laser beam.

On the other hand, at the Fraunhofer Institute für Werkstoff und Strahltechnik (IWS), the Metal Laminated Tooling Melato [6] process chain was established by critical edge finishing using laser deposition welding. A 430 x 430 mm tool was divided into modules according to its complexity, anchor-joined sheets were used for the most critical modules and subsequently the staircase effect was reduced by combining 5-axis milling and 3d laser cutting. The component was reinforced by applying laser build-up welding.

Furthermore, Geiger et al, applied deep drawing at 1 mm sheet to dies composed from cut sheets [7]. These had a maximum bevel of 25° using three-dimensional laser cutting and were joined by two different means: welding and sticking, thus obtaining 23 and 20 manufacturing hours respectively.

In the literature review [8] it was suggested that additive manufacturing processes could be implemented for complex geometries such as dies, since they have internal channels, with the disadvantage of low surface quality. It was suggested that final machining processes such as milling and eroding could be combined. One of these additive manufacturing processes that could be applied is laser direct metal deposition (LDMD), since it allows the use of different materials and the fusion of layers of these, initially in powder form, on a solid substrate [9]. The relative movement between the laser and the work surface results in a molten material track, and the repetition of the same, allows the production of complex volumes.

Nevertheless, it was found that the dimensions of a single track are influenced by many parameters, for example, its width increases with laser power and substrate temperature [10], but if tracks are built upon each other, the width decreases in the upper tracks [9], [11]. It was also found that the height of a single-track decreases with increasing transverse velocity [12]. Nevertheless, there is not enough information on the optimal parameters for multilayer processes.

Another factor is dilution which relates the molten bond, if this is too low, it indicates insufficient melting, but if too high, excessive melting [9]. This research also mentions the porosity due to lack of energy, oxide layers, trapped air or moisture. As for the surface finish, roughness is higher in the direction of construction than in the transverse direction [13]. In addition, components manufactured by LDMD have superior mechanical properties to typical annealed forgings [14]. However, they are anisotropic due to directional solidification, i.e. yield and ultimate tensile strengths are higher in the horizontal direction, but ductility is higher in the vertical direction (Pinkerton). As for residual stresses, they are produced due to the transient thermal gradient of the deposited material [15] and for their reduction, it has been proposed to preheat the substrate [16].

An investigation analyzed the effect of overlap in a single layer [17]. It used P420 stainless steel powder on an AISI 1018 substrate and analyzed microhardness, melt pool dimensions and geometry of the heat affected zone (HAZ) for 40%, 50% and 60% overlap. It was concluded that the microhardness is lower in the first tracks, especially near the substrate, but it is more uniform with a zigzag pattern. Also the subsequent tracks change the structure of the previous tracks, generating residual stresses and distortions and also, no ideal overlap was observed. One article investigated the shape by using three layers to build a thin wall [18]. The height at the ends was higher, possibly attributed to a higher temperature at these points. Another investigation studied deposition strategies in a layer with 50% overlap [19]. It was observed that the longitudinal zigzag strategy presented lower temperature peaks than transverse zigzag. It also presented less residual stress and therefore, less distortion. Another investigation studied the overlap of 50% and 70% for a single layer but with three tracks forming concentric circles. It concluded a strong influence of overlap and power on hardness and cooling rate [20]. Substrate inclination was investigated using alloy 718 for three different positions [21]. It is concluded that gravity and perpendicularity between the nozzle and substrate affect the shape of the track.

Hybrid manufacturing, combining laminated tools and metal powder deposition to reduce the staircase effect, could be a promising technology for manufacturing complex geometries such as dies. Nevertheless, it is required to identify the optimal parameters considering its surface finish and desired geometry. Therefore, in this research the reduction of the staircase effect in laminated component using 316L powder as deposition material and coaxial laser is studied. For this purpose, its optimum parameters are determined in order to achieve the lowest surface finish mechanically and optically. In addition, deposition strategies and sheet configuration are proposed to reach the desired geometry.

2. Materials and experiments preparation

As sheets are stacked to form a curvature, the staircase effect is observed, i.e. the sheets instead of completing the curvature, form a staircase profile. To achieve the desired curvature, material is added by metallic powder deposition whose properties are shown in Table 1. The material, the mechanical properties and chemical composition of the sheets to be stacked are shown in Table 2. The staircase effect reduction process consists of two stages: the sheet bonding step and the filling step. For the bonding of the sheets, the LDMD metal powder deposition is used and the optimum parameters established by Hamm (2020) are used. In that study, it is concluded that the best bonds, i.e., those parameters with which the highest shear strength is obtained for 316L, are 1400 W, mass flow: 7 g/min and feed rate: 1000 mm/min. Nevertheless, for the filling step there is limited documentation available. As a consequence, the optimum deposition parameters during the filling stage are determined in the present research by experiment.

Table 1. Deposition powder properties. Adapted from [22]

(a)

Material	Density at 20°C (g/cm3)	Melting point (°C)	Vickers hardness (HV)
316L	8.0	1400	225

(b)

Material	Ni (%)	Cr (%)	Mo (%)	Si (%)	Mn (%)	C (%)
316L	12	17.0	2.5	2.3	1.0	0.03

Table 2. Sheets properties (Knauf Interfer, Stahl Service Center): a) Mechanical properties, b) Chemical composition

(a)Material	E (GPa)	R_{p02} (MPa)	R_m (MPa)	A_{80} (%)
HC 420 LA	191	458	556	21.62

(b)

Material	C (%)	Si (%)	Mn (%)	P (%)	S (%)	Al (%)	Ti (%)	Nb (%)
HC 420 LA	0.1	0.5	1.6	0.025	0.025	0.015	0.15	0.09

Other parameter to be considered is the metal deposition patterns. The author [23] explore the raster, bi-directional, offset-out and fractal patterns, however, for this purpose, only the first pattern is considered (Figure 1a) since it is the most common strategy and less deflection in the part is obtain.

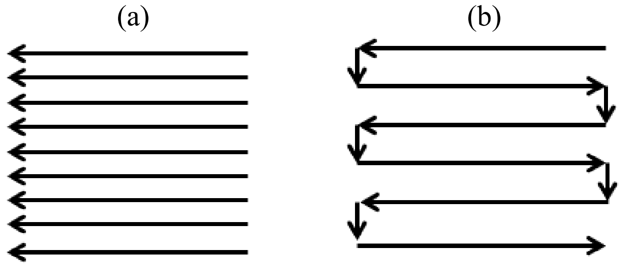

Figure 1. Different deposition patterns: (a) raster, (b) bi-directional *[23]*

The aspects to consider are the radius required to be formed, the sheet thicknesses to be used and the order of stacked sheets. Continuing with Hamm's previous work, the radius to be obtained is 14 mm and the sheet thicknesses are 0.5, 1 and 2 mm. The purpose of the 14 mm radius is to reproduce a hybrid-shaped deep-drawing die and its subsequent performance comparison with a conventionally manufactured one. The order of the sheets is represented through the thickness vector, which simply consists of setting the sequence from the upper sheet to the lower sheet. Table 3 and 4 show the characteristics of the two types of sheet arrangements to be used. For a better understanding, in these tables is also represented the illustration for the stacking of sheets whose depth is 50 mm. To achieve the desired curvature of 14 mm, the sheets are previously cut to different lengths (represented by the lengths vector), cleaned, measured, sorted and stacked. Also the yellow triangles correspond to the initial bonding step. Although an experiment is required to determine the optimal parameters for the filling step. Considering the above and taking into account that there are many possible combinations of sheets, it is decided to use a 2 mm thick sheet as the top sheet in order to have a maximum filling volume of 9.76 mm^2 (orange color). On the other hand, the effect with different substrates is analyzed, i.e., the second sheet has a thickness of 2 mm and 1 mm for the first and second arrangement respectively. The thicknesses of the remaining sheets are established without any specific criteria. For metal powder deposition by LDMD the Lasertec 65 3D machine is used, which is shown in Figure 2. This figure also shows how the sheets are stacked at 45° in order to facilitate programming. For programming the Catia V5 software is used to model the stacked sheets as a single part, its clamping assembly, the bonding step volumes (yellow color) and finally the filling step volume (orange color). The CAD models are then imported into the NX 12 software. The assembly corresponding to the Lasertec 65 3D machine is also imported there, considering the coaxial laser diameter of 1.6 mm. By means of the Freeform additive Buildup function, the G-code is generated.

Table 3. Characteristics of the first stack of sheets.

Thickness vector N°1 (mm)	2; 2; 2; 1; 1; 1; 1; 1; 0.5 ;0.5; 0.5; 0.5; 0.5; 0.5	
Length vector N°1 (mm)	36; 43.2;45.8; 47.5; 48.1; 48.6; 49.1; 49.4; 49.7; 49.8; 49.9; 49.9; 50.0; 50.0	
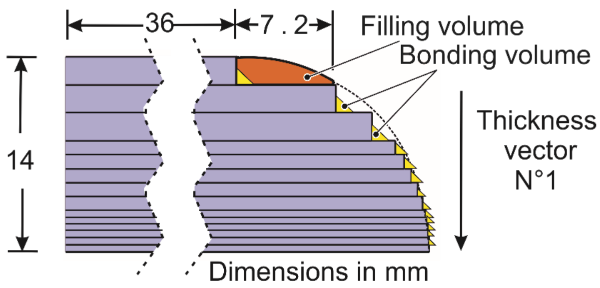	Radius (mm)	14
	Maximum total area (mm^2)	15.6
	Maximum area (mm^2)	9.76
	Total sheets number	14
	Sheet thickness under the area to be filled (mm)	2
Thicknesses of used sheets (0.5 mm / 1 mm / 2 mm) (%)	42.9/ 35.7/ 21.4	

Table 4. Characteristics of the second stack of sheets.

<table>
<tr><td>Thickness vector N°2 (mm)</td><td colspan="2">2; 1; 2; 1; 2; 1; 2; 1; 2;</td></tr>
<tr><td>Length vector N°2 (mm)</td><td colspan="2">36; 43.2; 44.7; 46.7; 47.5; 48.6; 49.1; 49.7; 49.9</td></tr>
<tr><td rowspan="5">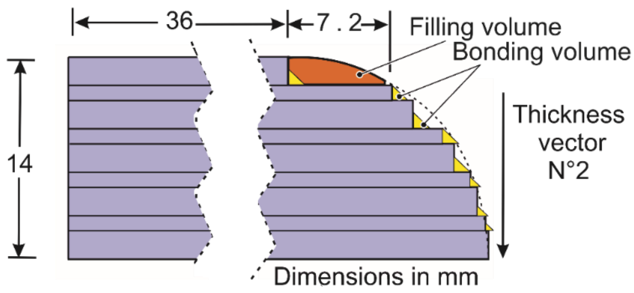
</td><td>Radius (mm)</td><td>14</td></tr>
<tr><td>Maximum total area (mm^2)</td><td>15.3</td></tr>
<tr><td>Maximum area (mm^2)</td><td>9.76</td></tr>
<tr><td>Total sheets number</td><td>9</td></tr>
<tr><td>Sheet thickness under the area to be filled (mm)</td><td>1</td></tr>
<tr><td colspan="2">Thicknesses of used sheets (0.5 mm / 1 mm / 2 mm) (%)</td><td>0/ 44.4/ 55.6</td></tr>
</table>

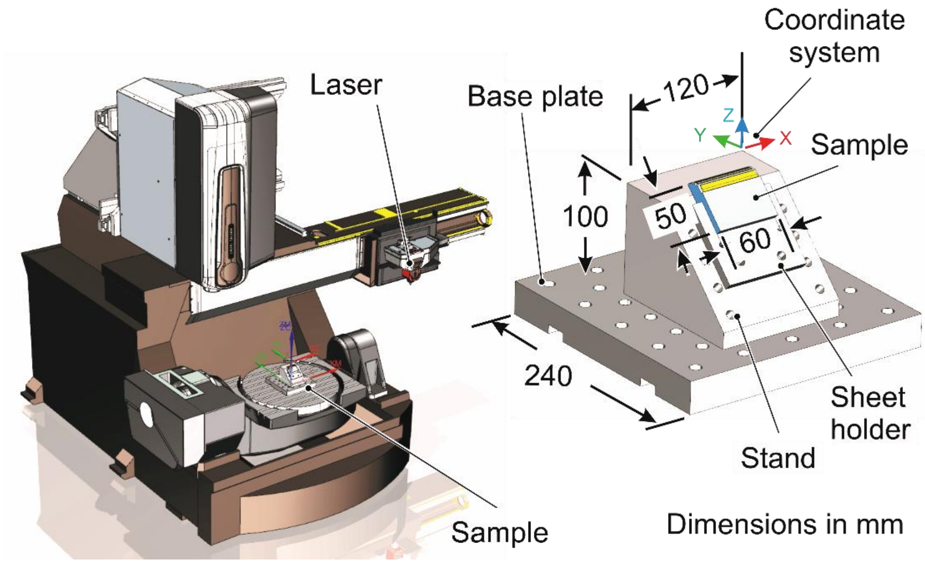

Figure 2. Experimental setup

3. Taguchi design of experiment (DOE)

Taguchi's method, as the design of experiments, is used to optimize parameters in a short time. Table 5 shows the parameters to be considered with their respective levels for 316L. It is important to clarify that during the filling step, tracks or paths of deposited material are built, but the overlap between them is another parameter to be investigated. Therefore, using the simulation tools of the NX 12 software, Figure 3 shows the volume to be filled, where each black dot corresponds to a track and the effect of the overlapping is observed. On the other hand, the volume to be filled is formed by a constant number of layers and these, in turn, are composed of a certain number of tracks. These parameters are kept constant in this research because it is not known if they are sufficient to achieve the desired profile. The number of layers and tracks are shown in Figure 4 as well as the principle of operation via the coaxial nozzle.

Table 5. Parameters and levels

Symbols and Parameters		Level 1	Level 2
-	Overlap (%)	35	55
t	Substrate thickness (mm)	1	2
P	Laser power (W)	500	1000
$\dot{m}$	Powder mass flow (g/min)	4	8
v	Feed rate (mm/min)	700	1400

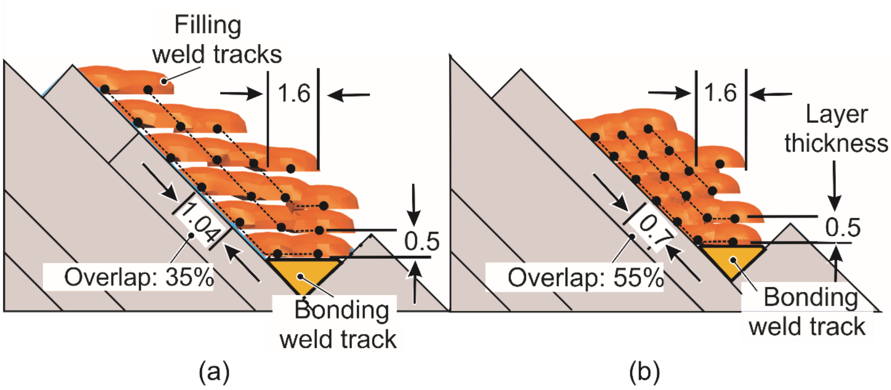

Figure 3. (a) Overlap: 35% (b) Overlap: 55%

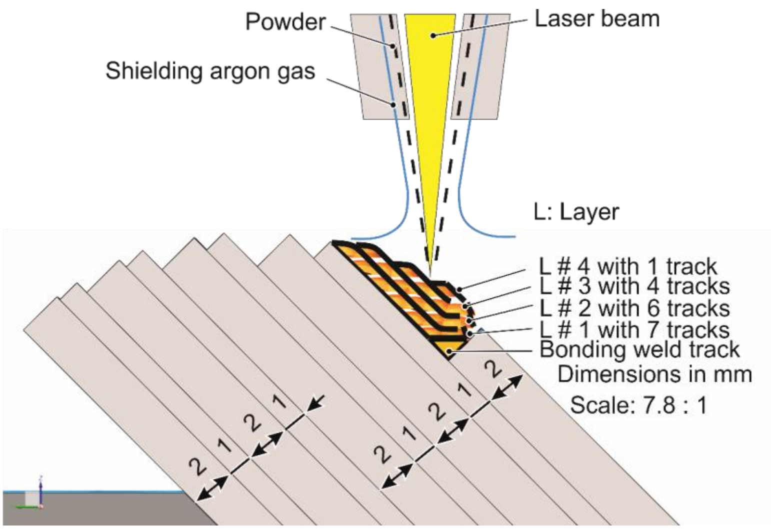

Figure 4. Layers that define the filling step and the number of tracks

The Taguchi L8 (2^4) orthogonal array is generated via Minitab. For each overlapping level, four parameters are considered and L8 experimental runs. Therefore, 16 experimental runs are performed: overlapping of 35% for experimental runs from 1 to 8 and overlapping of 55% for experimental runs from 9 to 16 as shown in Table 6. For each experimental run there are two replicates.

Table 6. Experimental layout L8 (2^4) for 316L

Trial	Parameters				
	Overlap	Substrate thickness	Power	Powder mas flow	Feed rate
	(%)	(mm)	(W)	(g/min)	(mm/min)
1/9	35/55	1	500	4	700
2/10	35/55	1	500	8	1400
3/11	35/55	1	1000	4	1400

Trial	Parameters				
	Overlap	Substrate thickness	Power	Powder mas flow	Feed rate
	(%)	(mm)	(W)	(g/min)	(mm/min)
4/12	35/55	1	1000	8	700
5/13	35/55	2	500	4	1400
6/14	35/55	2	500	8	700
7/15	35/55	2	1000	4	700
8/16	35/55	2	1000	8	1400

4. Mechanical roughness and height deviation analysis

It is not just reducing the staircase effect that is important, also the surface roughness is important. It is measured mechanically using the Marsurf GD26 machine shown in Figure 5. Its principle is based on a probe arm that makes vertical contact with the surface and moves horizontally 16 mm while saving the roughness profile information. Additionally, the reference point is set using the MarWin easy roughness software, as well as the drive unit (GD26 MI 500(#1101)) and the test arm (BFW A 10-45-2/90) are selected. Finally, the measuring range has a granular wavelength λ_c of 8 mm and, according to DIN EN ISO 4288, the final surface is quite rough with the range of 50 to 200 µm for R_z and 10 to 80 µm for R_a.

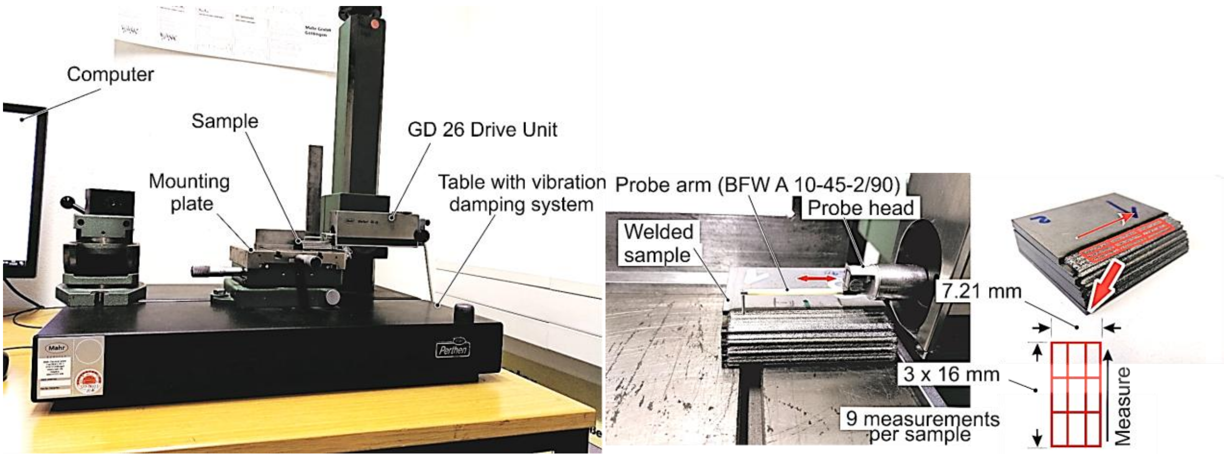

Figure 5. Mechanical Roughness Measurement Unit

5. Optical roughness measurement

The NanoFocus µsurf explorer microscope additionally provides an optical analysis of the samples. For each sample an image of 6.075 mm x 7.425 mm is generated, i.e. a small image is taken from the middle of the surface of each sample as shown in Figure 6. An 800-L lens (20x long) is also used due to the curved surface and step motor mode. The parameters to be analyzed are classified into height parameters and functional parameters. The height parameters are S_a, S_z, S_{sk}, S_{ku}, S_p, S_v, R_a and R_z while the functional parameters are S_{mr1}, S_{pk} and S_{vk}. R_a and S_a. R_z and S_z are the sum of the height of the maximum peaks and maximum deep valleys. S_p is the maximum peak that will be used in a sliding application. S_v is the maximum valley depth. On the other hand, Skewness S_{sk} and kurtosis S_{ku}, characterize the shape and distribution of the surface height with respect to the mean plane (DIN ISO 25178). In case $S_{sk} > 0$ indicates a peaks prevalence, whereas $S_{sk} < 0$ indicates a valleys predominance on the surface and great sliding surface. In other words, as a load is applied to the surface, less peaks are in contact and therefore, less wear. On the other hand, the lubricant is retained by the deep valleys improving lubrication [24].

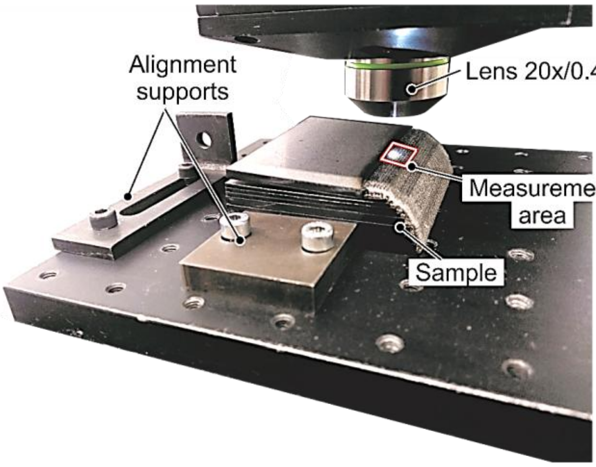

Figure 6. Microscope setup

6. Residual stress measurement

In order to measure the residual stresses of the surface, the non-destructive method based on X-ray diffraction is used. As shown in Figure 7, on the additive surface as well as on the upper sheet, three points are measured (at the beginning, in the middle and at the end of each track) and two measurement directions are considered. The calibration parameters are: material: Fe ferrite, exposure time: 5 s, N ° of tilts: 5/5, tilt angle: + -42, tilt oscillation: 3, threshold: 8 MPa, collimeter: 2mm. The parameters for measuring 316L as deposited material are collimeter diameter 2mm, exposure time: 20 s, N ° of tilts: 5/5, tilt angle: - + 42. tilt oscilation: 3, 2theta: 152.3, X-ray tube type: Cr. The parameters for measuring the residual stresses in the sheet are: Exposure time: 7 s, N ° of tilts: 7/7, tilt angle: + -42, tilt oscillation: 3, 2theta: 156.4.

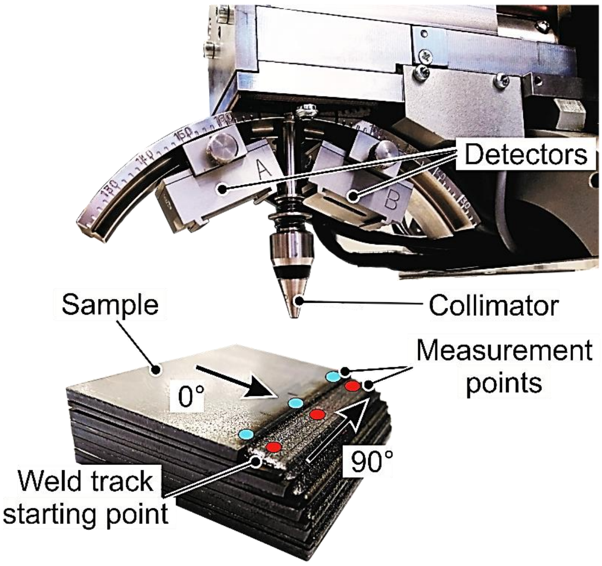

Figure 7. X-ray diffraction setup

7. Results and Discussion

7.1. Mechanical roughness analysis and height deviation

An experiment was performed: 16 experimental runs with two replicates were run using 316L as deposition material. In Figure 8 one of the samples with 316L is shown. A separation in the back sheets was observed, which is called height deviation Δh and was analyzed in each experimental run. Also, high roughness (> 300 µm) was observed for the experimental runs 2, 5, 10 and 13.

Figure 8. Height deviation Δh and welded sample with high roughness for 316L

The main effect plot for the arithmetic roughness R_a and for the maximum roughness R_z for 316L is shown in Figure 9. In addition, the main effect plot for the height deviation Δh is shown in Figure 10. This type of plots allows to determine if a parameter contributes significantly to the response, i.e., if the level of overlap, substrate thickness, power, mass flow and feed rate contribute significantly to the roughness R_a and R_z and the height deviation Δh. For each parameter and at each level, the roughness and height deviation values were averaged, and these average values were connected by a line. If the resulting line is steep, it means that the parameter contributes significantly to the response, but if the resulting line is horizontal, it means that the parameter contributes little or is still within its optimum value. As shown in Figure 9, the parameter that contributes most to both the arithmetic roughness R_a and maximum roughness R_z, i.e., the steepest line, is the laser power (42.91%). The second most contributing parameter is the substrate thickness (32.54%). The least contributing parameter is the overlap (1.04%).

In the case of height deviation Δh, the feed rate (36.91%) and substrate thickness (32.05%) have a great influence, as shown in Figure 10. Nevertheless, the mass flow (5.07%) and the overlap (4.51%) have a low influence. In contrast to the roughness response, laser power has a minor contribution (21.46%). In other words, it is concluded that a lower roughness was obtained at higher laser power, higher mass flow and higher feed rate. But the higher laser power, the higher deviation. It should be noted that the overlap has low influence on both roughness and height deviation.

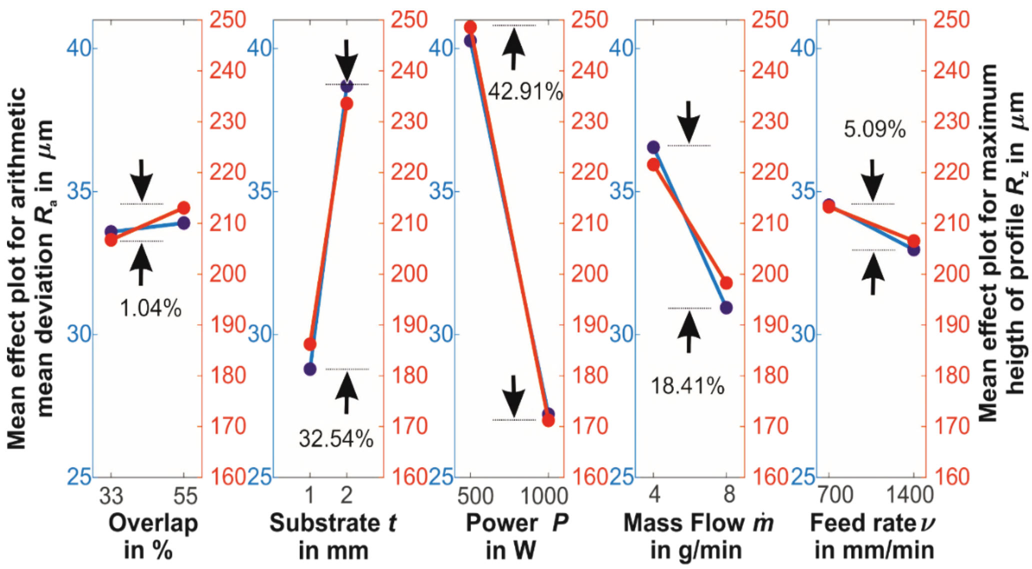

Figure 9. Main effect plot for mean roughness R_a and R_z for 316L

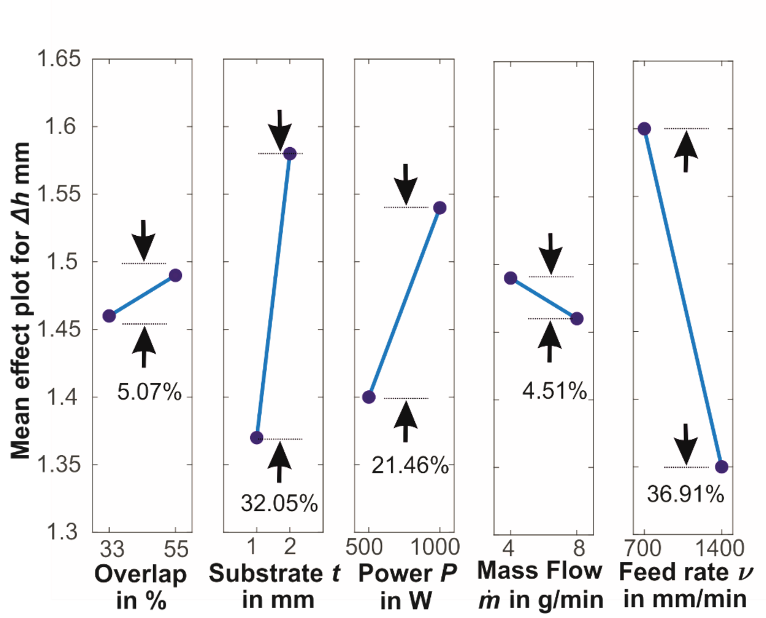

Figure 10. Mean effect plot for mean height deviation Δh for 316L

7.2. Optical roughness analysis

Because of the time consumption, the best experimental runs were selected, i.e., those with low roughness measured mechanically. These correspond to experimental run 3, 8, 11 16. Through microscope an image 6.13 mm x 7.21 mm per sample was obtained as shown in Figure 11 c). The height parameter results are shown in Figure 11 a). It was concluded that at constant overlap and few mass flow, the arithmetic mean deviation R_a and the maximum peak profile R_z decreased, also for S_z, S_p and S_a as well. As a second observation, at 4 g/min mass flow, as overlap increased, S_z decreased, but at 8 g/min mass flow, S_z increased. On the other hand, the functional parameters are shown in Figure 11 b). S_{pk} decreases and in turn, the contact stresses, by increasing mass flow and overlap. In addition, the lubricant holding capacity improves with increasing valley depth S_{vk}, i.e., with increasing mass flow. Finally, there is slip capacity in all samples due to negative S_{sk}. However, the surface is characterized as spiked, i.e., $S_{ku} > 3$, which is a consequence of the adhesion of particles from the dust cloud during processing. For high mass flow, the spiked surface decreases.

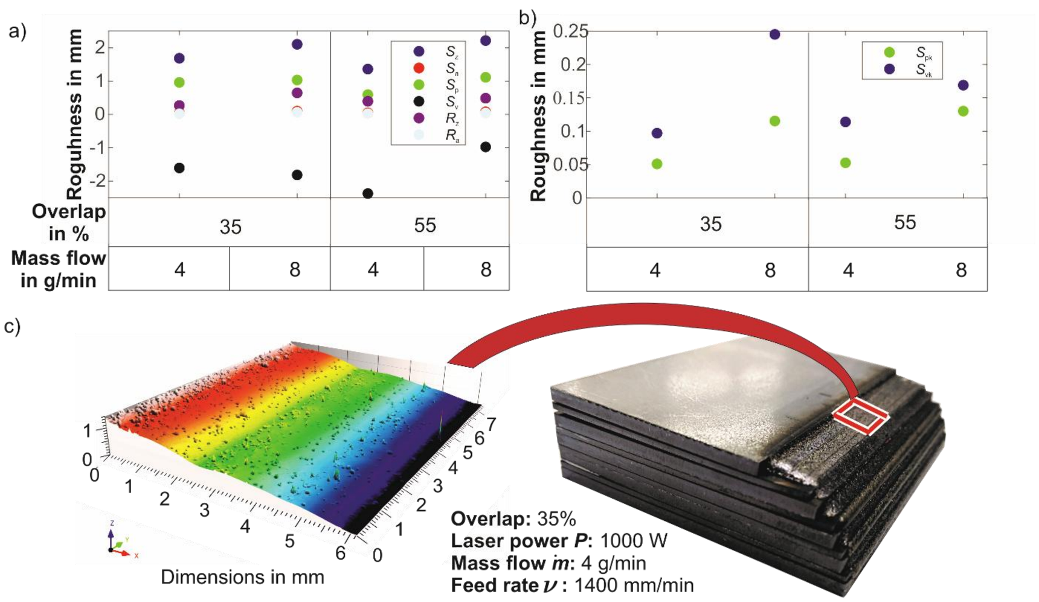

Figure 11. Optical roughness for 316L: a) Height parameters b) Functional parameters c) Microscope image for sample with overlap 35%, power 1000W and 4 g/min

7.3. Residual stress analysis

Near-surface residual stresses were analyzed by X-ray diffraction. As in the optical microscopy analysis, due to the time consumption and measurement complexity, the same four experimental runs were analyzed (3, 8, 11 and 16). By observing the graph, residual tensile stresses (positive residual stresses) were obtained, which is due to the rapid heating-cooling cycles that occur in additively manufactured components. This type of stresses is undesirable since they adversely affect the fatigue strength. In addition, in these thermal cycles, the material expands due to the laser heating, nevertheless, this expansion is restricted by the surrounding material generating compression zones [25]. As the laser is removed, the cooling stage takes place and the former zones shrink and are partially restrained by the plastic deformation previously developed and thus, generating tensile stresses. When having multi-layer additive manufacturing, tensile stresses increase due to the presence of more cycles with remelting and re-solidification processes. It was also observed that residual stresses decreased in both directions as mass flow increased. This occurs because the higher the mass flow, the more material expansion and the higher the compressive stresses. Then, in the cooling stage, tensile residual stresses are formed which are lower due to the higher initial compressive stresses. This also explained with the overlap, since the lower the overlap, the lower the residual stress in tension due to better spacing of the material and less restriction of the shrink during cooling.

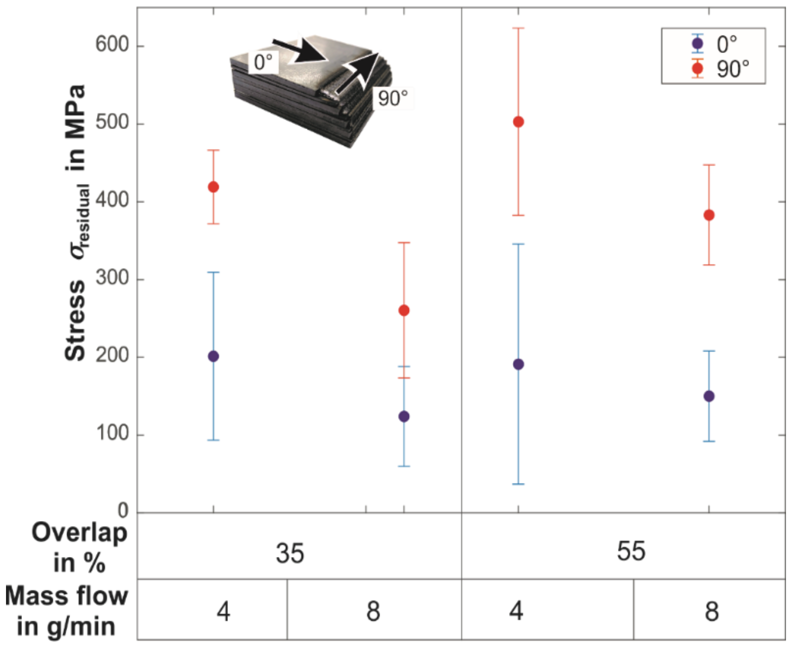

Figure 12. Mean residual stress of the experimental run with lower roughness for 316L

Figure 13 shows the stresses obtained for experimental run 3 at the three measurement points at both 0° and 90°. These are dominated by tensile residual stresses and a parabolic shape that is in accordance with the research of Moat et al [26]. This could be due to the fact that at the extremes, cooling is at a lower rate, because of their contact with the air, i.e., heat transfer by conduction is lower, while in the middle, there is greater heat conduction. Regarding the effect of position, residual stresses are higher at 90° than at 0°. The reason for this is the anisotropy presented due to directional solidification [27] since the material has been deposited at 90°, leading to thermal cycling and residual stresses in this direction. To reduce the residual stresses Liu et al [28], suggests preheating the substrate to increase the temperature gradient. Also this can be noticed by comparing the end points. The residual stresses are higher at the starting point than at the end point because when the laser reaches the end point, the substrate is already preheated because it has absorbed heat during the previous process. The residual stresses in the upper sheet at 90° also showed a parabola as shown in Figure 14, i.e., the residual tensile stresses were higher in the middle. But at 0° the residual stresses were not affected by the process since they were compressive residual stresses.

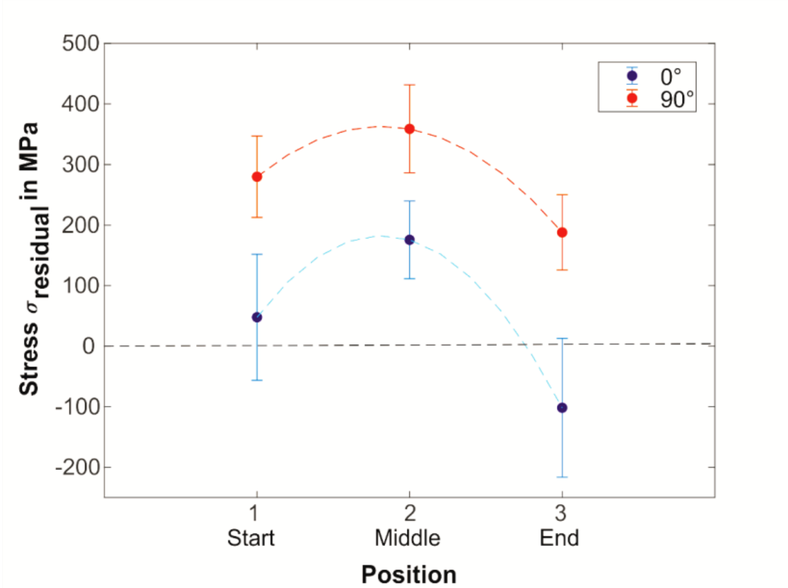

Figure 13. Residual stress in deposited or welded material for the sample with 316L as deposition material and 35% overlap, 1000 W, 4 g / min, 1400 mm/min as parameters (experimental run 3)

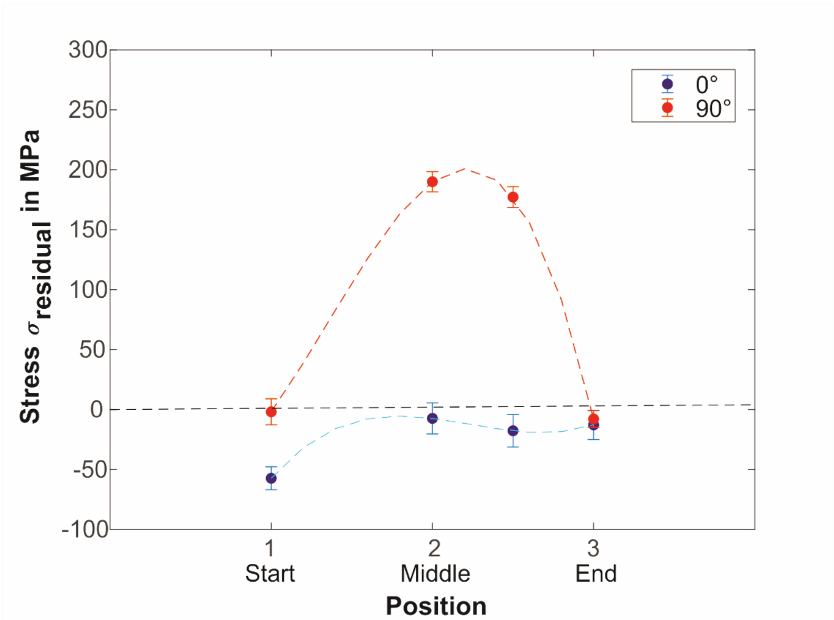

Figure 14. Residual stress in the upper sheet for experimental run 3

8. Conclusion and outlook

The reduction of the staircase effect in laminated parts was achieved using LDMD with 316L powder as the deposition material. Nevertheless, this process involved many parameters, requiring an experiment to determine the optimal parameters for lower roughness. Based on three different sheet thicknesses (0.5, 1, and 2 mm), two sequences or vectors of thicknesses were made, forming a curvature of 14 mm and 50 mm in depth. The upper area of the sheets was decided as the most suitable for multilayer deposition because it had enough space. Based on mechanical measurements, the optimal parameters for achieving the lowest roughness using 316L as the deposition material were: low overlap, mass flow, and substrate thickness: 35%, 4 g/min, and 1 mm, respectively; high laser power and feed rate: 1000 W and 1400 mm/min, respectively. On the other hand, a separation of the upper sheets was observed, leading to a change in the component height, which was called height deviation Δh. To obtain the lowest deviation, low laser power and high feed rate were required.

However, due to the limitation of mechanically measured roughness for very high roughness values (< 250 μm), only the best samples were analyzed with an optical microscope, finding that the peak height decreases as the mass flow decreases and the feed rate increases, which favors sliding. Furthermore, residual stresses were measured using XRD in the longitudinal (90°) and transverse (0°) directions. Due to the high cooling rates, the surface of the additive volume was subject to tensile residual stresses, which affect fatigue. In addition, these stresses were greater in the longitudinal direction because this is the direction of construction and solidification, which produces anisotropy. Comparing the starting and ending points of the track, the starting point had greater residual stress because it had a higher temperature gradient, since the substrate was initially at room temperature. The midpoint of each track had the highest residual stresses at high cooling rates, since this area experienced greater heat transfer by conduction because it was surrounded by material. Finally, coaxial laser metal powder deposition technology is useful for reducing the staircase effect in laminated parts. However, research is needed into ways of reducing both residual tensile stresses and roughness, either by preheating the sheets or applying post-processing techniques. For future work, strategies must be developed to achieve the required contour and study different deposition directions and angles between the laser and the substrate.

Declaration of competing interest

The authors declare that they have no any known financial or non-financial competing interests in any material discussed in this paper.

Funding information

No funding was received from any financial organization to conduct this research.

References

[1] J. F. Pritchard, "Interlaminate strength of laminated die tooling," Iowa State University, Digital Repository, Ames, 2010. doi: 10.31274/etd-180810-1554.

[2] D. F. Walczyk and D. E. Hardt, "Recent Developments in Profiled-Edge Lamination Dies for Sheet Metal Forming," 1996, doi: 10.15781/T2D795W86.

[3] D. F. Walczyk and S. Yoo, "Design and fabrication of a laminated thermoforming tool with enhanced features," *J Manuf Process*, vol. 11, no. 1, pp. 8–18, Jan. 2009, doi: 10.1016/j.jmapro.2009.04.003.

[4] S. H. Yoon and S. J. Na, "Rapid Laminated Tooling by a Brazing and Soldering Process," *J Manuf Process*, vol. 5, no. 2, pp. 118–126, Jan. 2003, doi: 10.1016/S1526-6125(03)70047-4.

[5] S. H. Yoon and S. J. Na, "Application of laser joining process for elimination of stair steps in steel laminate tooling," *The International Journal of Advanced Manufacturing Technology*, vol. 25, no. 1–2, pp. 154–159, Jan. 2005, doi: 10.1007/s00170-003-1815-7.

[6] T. Himmer, A. Techel, S. Nowotny, and E. Beyer, "Recent developments in metal laminated tooling by multiple laser processing," *Rapid Prototyp J*, vol. 9, no. 1, pp. 24–29, Mar. 2003, doi: 10.1108/13552540310455629.

[7] M. Geiger, M. Euringer, R. Neugebauer, and F. Garreis, "Lamellierte Aktiv-Werkzeugelemente in flexiblen Blechumformwerkzeugen," *Blech Rohre Profile 1/2*, pp. 34–37, 1999.

[8] R. Hölker-Jäger and A. E. Tekkaya, "Additive manufacture of tools and dies for metal forming," in *Laser Additive Manufacturing*, Elsevier, 2017, pp. 439–464. doi: 10.1016/B978-0-08-100433-3.00017-8.

[9] A. J. Pinkerton, "Laser direct metal deposition: theory and applications in manufacturing and maintenance," in *Advances in Laser Materials Processing*, Elsevier, 2010, pp. 461–491. doi: 10.1533/9781845699819.6.461.

[10] W. Hofmeister and M. Griffith, "Solidification in direct metal deposition by LENS processing," *JOM*, vol. 53, no. 9, pp. 30–34, Sep. 2001, doi: 10.1007/s11837-001-0066-z.

[11] A. Vasinonta, J. L. Beuth, and M. L. Griffith, "A Process Map for Consistent Build Conditions in the Solid Freeform Fabrication of Thin-Walled Structures," *J Manuf Sci Eng*, vol. 123, no. 4, pp. 615–622, Nov. 2001, doi: 10.1115/1.1370497.

[12] M. A. McLean, G. J. Shannon, and W. M. Steen, "Laser generating metallic components," Apr. 1997, p. 753. doi: 10.1117/12.270181.

[13] H. Ki, J. Mazumder, and P. S. Mohanty, "Modeling of laser keyhole welding: Part I. mathematical modeling, numerical methodology, role of recoil pressure, multiple reflections, and free surface evolution," *Metallurgical and Materials Transactions A*, vol. 33, no. 6, pp. 1817–1830, Jun. 2002, doi: 10.1007/s11661-002-0190-6.

[14] J. E. Smugeresky, D. M. Keicher, J. A. Romero, M. L. Griffith, and L. D. Harwell, "Using the Laser Engineered Net Shaping (LENS{trademark}) process to produce complex components from a CAD solid model," Albuquerque, NM, and Livermore, CA (United States), Aug. 1997. doi: 10.2172/554822.

[15] Y. C. Tsui and T. W. Clyne, "An analytical model for predicting residual stresses in progressively deposited coatings Part 1: Planar geometry," *Thin Solid Films*, vol. 306, no. 1, pp. 23–33, Aug. 1997, doi: 10.1016/S0040-6090(97)00199-5.

[16] J. Beuth and N. Klingbeil, "The role of process variables in laser-based direct metal solid freeform fabrication," *JOM*, vol. 53, no. 9, pp. 36–39, Sep. 2001, doi: 10.1007/s11837-001-0067-y.

[17] N. Nazemi, J. Urbanic, and M. Alam, "Hardness and residual stress modeling of powder injection laser cladding of P420 coating on AISI 1018 substrate," *The International Journal of Advanced Manufacturing Technology*, vol. 93, no. 9–12, pp. 3485–3503, Dec. 2017, doi: 10.1007/s00170-017-0760-9.

[18] Y. Huang, M. B. Khamesee, and E. Toyserkani, "A new physics-based model for laser directed energy deposition (powder-fed additive manufacturing): From single-track to multi-track and multi-layer," *Opt Laser Technol*, vol. 109, pp. 584–599, Jan. 2019, doi: 10.1016/j.optlastec.2018.08.015.

[19] K. Ren, Y. Chew, J. Y. H. Fuh, Y. F. Zhang, and G. J. Bi, "Thermo-mechanical analyses for optimized path planning in laser aided additive manufacturing processes," *Mater Des*, vol. 162, pp. 80–93, Jan. 2019, doi: 10.1016/j.matdes.2018.11.014.

[20] F. Mazzucato, A. Aversa, R. Doglione, S. Biamino, A. Valente, and M. Lombardi, "Influence of Process Parameters and Deposition Strategy on Laser Metal Deposition of 316L Powder," *Metals (Basel)*, vol. 9, no. 11, p. 1160, Oct. 2019, doi: 10.3390/met9111160.

[21] P. Ramiro-Castro, M. Ortiz, A. Alberdi, and A. Lamikiz, "Effects of Gravity and Non-Perpendicularity during Powder-Fed Directed Energy Deposition of Ni-Based Alloy 718 through Two Types of Coaxial Nozzle," *Metals (Basel)*, vol. 10, no. 5, p. 560, Apr. 2020, doi: 10.3390/met10050560.

[22] P. Meier and A. Rubrecht, "Space Materials Database."

[23] A. Saboori, D. Gallo, S. Biamino, P. Fino, and M. Lombardi, "An Overview of Additive Manufacturing of Titanium Components by Directed Energy Deposition: Microstructure and Mechanical Properties," *Applied Sciences*, vol. 7, no. 9, p. 883, Aug. 2017, doi: 10.3390/app7090883.

[24] B. Sagbas, "Post-Processing Effects on Surface Properties of Direct Metal Laser Sintered AlSi10Mg Parts," *Metals and Materials International*, vol. 26, no. 1, pp. 143–153, Jan. 2020, doi: 10.1007/s12540-019-00375-3.

[25] J. L. Bartlett, B. P. Croom, J. Burdick, D. Henkel, and X. Li, "Revealing mechanisms of residual stress development in additive manufacturing via digital image correlation," *Addit Manuf*, vol. 22, pp. 1–12, Aug. 2018, doi: 10.1016/j.addma.2018.04.025.

[26] R. J. Moat, A. J. Pinkerton, L. Li, P. J. Withers, and M. Preuss, "Residual stresses in laser direct metal deposited Waspaloy," *Materials Science and Engineering: A*, vol. 528, no. 6, pp. 2288–2298, Mar. 2011, doi: 10.1016/j.msea.2010.12.010.

[27] A. J. Pinkerton, "Laser direct metal deposition: theory and applications in manufacturing and maintenance," in *Advances in Laser Materials Processing*, Elsevier, 2010, pp. 461–491. doi: 10.1533/9781845699819.6.461.

[28] C. Li, Z. Y. Liu, X. Y. Fang, and Y. B. Guo, "Residual Stress in Metal Additive Manufacturing," *Procedia CIRP*, vol. 71, pp. 348–353, 2018, doi: 10.1016/j.procir.2018.05.039.